JOURNAL OF GEOPHYSICAL RESEARCH, VOL. 99, NO. B12, PAGES 24,039–24,050, DECEMBER 10, 1994

Dikes emplaced into fractured basement, Timna Igneous Complex, Israel

Gidon Baer and Michael Beyth
Geological Survey of Israel, Jerusalem, Israel

Ze'ev Reches
Department of Geology, Hebrew University, Jerusalem, Israel

Abstract. Dikes are usually envisioned as arrays of parallel segments dilated perpendicular to the direction of the least compressive stress. We describe here four dikes of highly irregular shape intruded in the fractured basement in the Timna Igneous Complex, southern Israel. The dikes include a doleritic dike, 2.3 km long and 1.6 m to 32 m thick, and three andesitic dikes, up to 1.5 km long and 8 m thick. The dikes each display significant variations of dip (up to 60°), strike (up to 160°) and thickness. The thickness variations correlate better with the segment attitude than with the position along the dikes. We show that the irregular shapes of the Timna dikes are the result of emplacement into fractured host rock under different paleostress states and driving pressures. Three dilation styles that differ by the geometry of the initial cracks are analyzed: an array of randomly oriented cracks (style A), a single linear crack (style B), and an array of interconnected, nonparallel cracks (style C). The analysis of style A provides the stress state during dike emplacement, including the orientations of the three principal stresses ($\sigma_1 \geq \sigma_2 \geq \sigma_3$), the stress ratio $\phi = (\sigma_2 - \sigma_3)/(\sigma_1 - \sigma_3)$, and the normalized driving pressure $R = (P_m - \sigma_3)/(\sigma_1 - \sigma_3)$. The stress ratio ϕ indicates the shape of the stress ellipsoid and it ranges from $\phi = 0$ for $\sigma_2 = \sigma_3$ (prolate ellipsoid) to $\phi = 1$ for $\sigma_1 = \sigma_2$ (oblate ellipsoid). The normalized driving pressure R indicates the relative magnitude of the internal magma pressure P_m with respect to the tectonic stresses, and it ranges from $R = 0$ for $P_m = \sigma_3$ to $R = 1$ for $P_m = \sigma_1$. We found that for three dikes in Timna, $\phi \sim 0.25$, indicating small differences between the two horizontal principal stresses, and for one dike $\phi \sim 0.9$, indicating a large difference between the two horizontal principal stresses. The normalized driving pressure R is about 0.08 in two horizontally propagating dikes and about 0.25 in two vertically propagating dikes. Style B predicts an elliptical thickness profile along the dike due to dilation of a linear crack; this prediction agrees with the profile of one of the dikes. The predicted thicknesses due to dilation of the interconnected array of cracks (style C) are in good agreement with the thickness variations of the doleritic dike, and in fair agreement with two of the andesitic dikes. Deviations from the ideal geometry suggest separate stages of propagation and dilation in some of the dike segments.

Introduction

Shapes of dikes can be strongly affected by the mechanical properties of their host rocks. A dike intruding a uniform rock usually creates its own fracture normal to the direction of the least compressive stress [*Anderson,* 1951] and dilates to an elliptical cross section [*Pollard,* 1973]. However, only seldom do dikes dilate a single fracture. They are generally comprised of an array of subparallel segments and fingers with shapes that depend on the host-rock lithology, stress field, and presence of preexisting fractures [*Pollard et al.,* 1975; *Baer and Beyth,* 1990; *Baer,* 1991]. Dikes often intrude host rocks with preexisting fractures not necessarily related to the contemporaneous regional stresses. *Delaney et al.* [1986] demonstrated how to distinguish between dike-generated fractures, that may serve as stress indicators, and preexisting fractures. They also showed how strike variations along dikes may indicate the ratio of magmatic to tectonic stresses under plane-strain conditions.

Paper number 94JB02161.
0148-0227/94/94JB-02161$05.00

We describe four dikes that intrude the fractured basement in the Timna Igneous Complex, southern Israel (Figure 1) and display significant attitude and thickness variations. We first describe these variations and show a detailed map of one dike to resolve the relationships between the dike and the host rock fractures. The three-dimensional stress state and the driving pressure associated with the emplacement of these dikes are then determined by analysis of the attitude variations of the cracks dilated by magma in each dike. Finally, we compare thickness variations along the dikes with thickness variations predicted for the dilation of idealized crack arrays.

Dikes in Timna Mountain

Field Description

Timna Mountain is an uplifted block at the margin of the Dead Sea rift, exposing plutonic and hypabyssal rocks of Late Precambrian age (Figure 1) [*Kroner and Beyth,* 1990]. The block is bounded by faults and is also crossed by several NW and N trending faults. Plutonic rocks in Timna include granite, olivine-norite, monzodiorite, and syenite [*Bentor,* 1961; *Zlatkine and Wurzburger,* 1957]. Hypabyssal rocks include

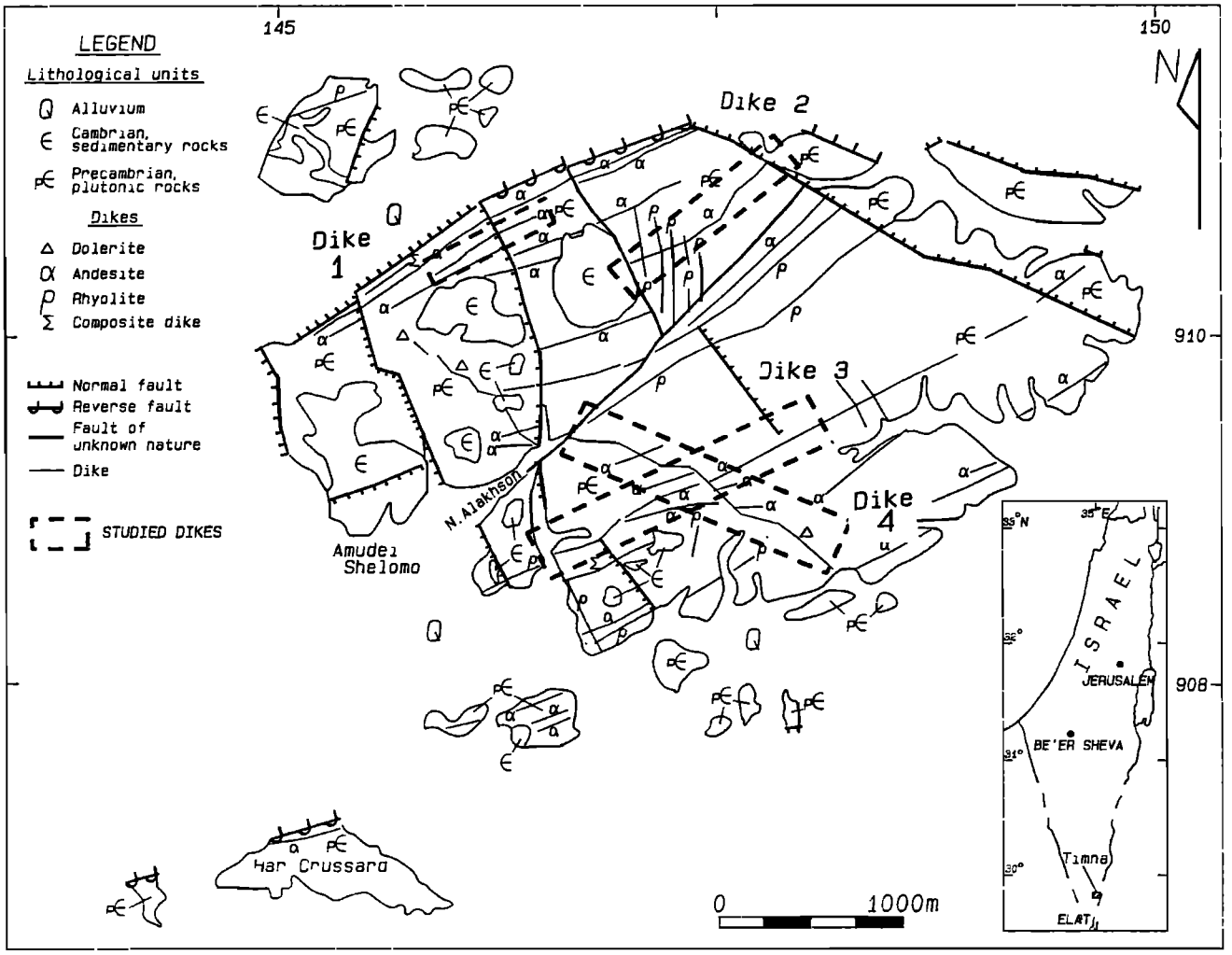

Figure 1. Location map of the dikes in Timna Mountain [modified after *Beyth et al.*, 1990].

rhyolitic, andesitic, and doleritic dikes [*Beyth and Peltz*, 1992], arranged in three dominant systems of decreasing relative age (Figure 1): N trending rhyolites, NE trending rhyolites and andesites (the rhyolites are generally older than the andesites), and NW trending dolerites. Dikes of the two younger systems, and in particular, the NE striking dikes, form regional swarms. They are abundant in other Precambrian outcrops south of Timna, in the Elat and Sinai regions [e.g., *Shafranek*, 1978], and extend as far west as the Eastern Desert in Egypt [*Schurmann*, 1966], and as far east as northern Saudi Arabia [*Vail*, 1970].

We mapped in detail and measured portions of four dikes (Figure 1): three NE trending andesitic dikes (dikes 1-3), and one NW trending doleritic dike (dike 4). Rhyolitic dikes are not well preserved and were thus excluded from the present analysis.

The NE trending dikes (dikes 1-3). These dikes parallel a regional system of joints (Figure 2a). Structures along two of these dikes (1 and 3) reveal subhorizontal steps, segment boundaries, ridges, and grooves (Figure 2b), indicating subhorizontal propagation according to *Pollard et al.* [1975] and *Baer* [1991]. Contact structures along dike 2 indicate subvertical propagation.

Dike 1 is about 600 m long and its thickness ranges from 0.5 m to 3 m, thinning towards both ends (Figure 3a). The dike is not truncated by faults and its exposed terminations are apparently close to the actual terminations. Dips of the dike segments vary from 55^0 to 85^0; dip directions range from 114^0 to 180^0 (degrees from north), with the majority dipping 70^0-75^0 to 140^0-150^0 (Figure 4a). The thickness of the dike segments appears to be related to their orientation, thinning from 2.5-3 m in 50^0-striking segments to 1-1.5 m in the 24^0- and the 90^0-striking segments (Figure 4a).

Dike 2 is about 1000 m long and its thickness varies from 3 m to 7 m, thinning towards its western end (Figure 3b). It is truncated by faults at both ends, and thus its exposed terminations are not necessarily the actual terminations. The orientation of the dike segments change along its course with segments dipping 75^0-90^0 to 140^0-150^0 more frequent (Figure 4b). The thicknesses of the segments do not display a clear correlation with their orientations (Figure 4b).

Dike 3 is about 2.5 km long and is not continuously exposed. Only its southwestern part was studied, and the measurement sites are more widely spaced with respect to the other three dikes. Thickness of the segments varies from about 4 m to 8 m (Figure 3c). As in the other dikes, attitudes of the dike segments vary (Figure 4c). The segments thin gradually from the thickest with dip and dip direction of 55^0 /150^0 to the thinnest dipping 80^0 /168^0 (Figure 4c).

The NW trending dike (dike 4). Dike 4 is about 2.3

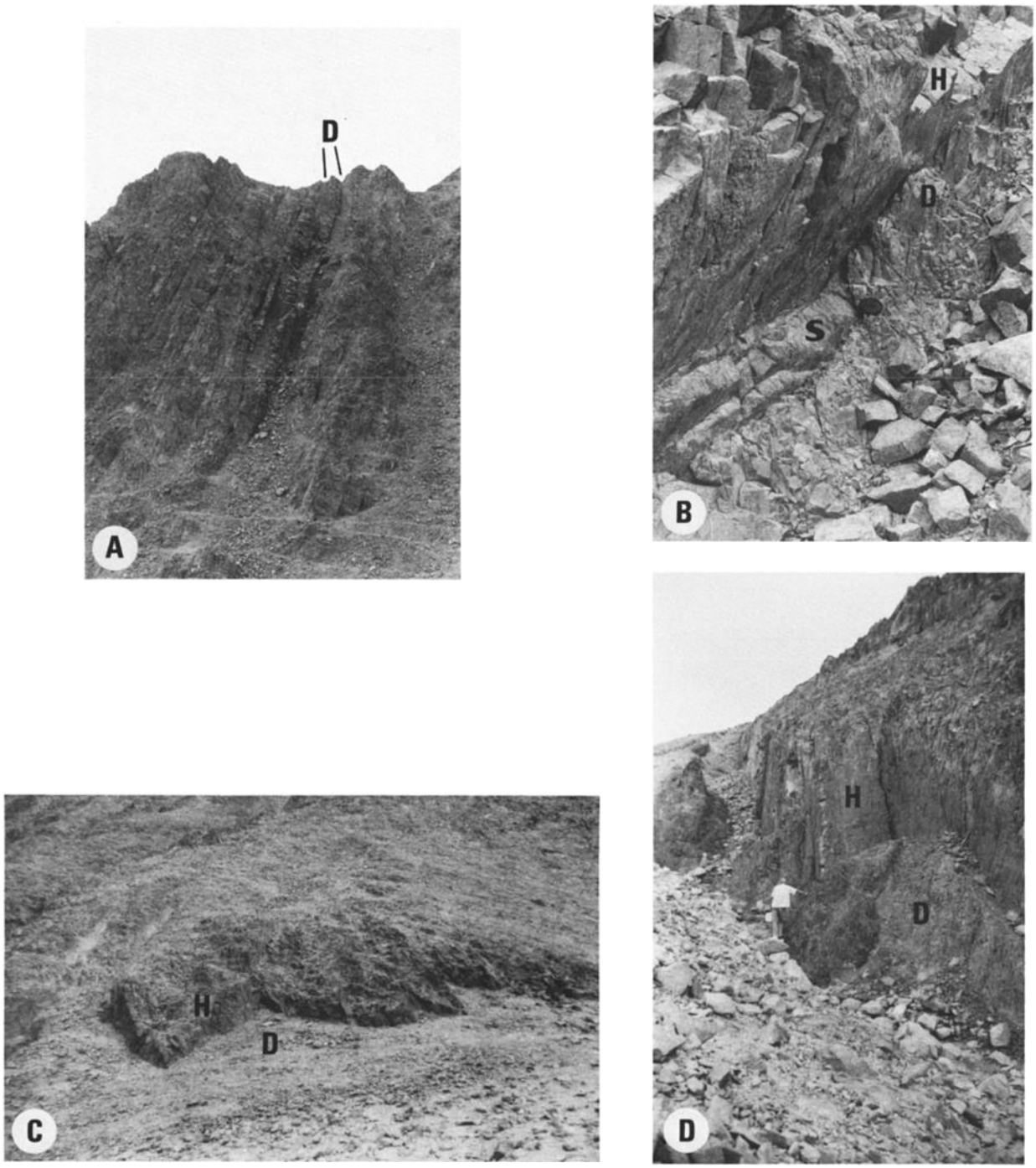

Figure 2. The Timna dikes and related structures (D, dike; H, host rock; S, step). (a) NE striking andesitic dikes and dike-parallel joints. (b) Subhorizontal steps at segment boundaries in dike 1, indicating a subhorizontal propagation direction. (c) Zigzag walls at the contact between dike 4 and the host granite at the northwestern end of segment 4 (area A in Figure 5). (d) Zigzag walls at the central part of dike 4 (area B in Figure 5).

km long; only its southeastern part (1.4 km long) was studied in detail due to poor exposures elsewhere. The general trend of this portion is 110^0-120^0 and it can be divided into six major sections (Figure 5): sections 2, 4 and 6 which strike 130^0-150^0 and sections 1, 3 and 5 which strike 60^0-85^0. Thickness varies from 1.6 m to 32 m (Figure 3d). The greater thicknesses correspond to the NW striking sections (Figures 5, 4d). This dike crosscuts the earlier swarm of NE striking dikes; the NW striking sections of dike 4 are left-stepped across the NE striking sections and terminate bluntly against them (Figure 5). The long axes of the section boundaries are subvertical (Figures 2c, 2d), suggesting that the dike propagated subvertically.

The walls of the six major dike sections are composed of more than 300 short offset segments that range in length from 0.1 to 30 m. These segments form a zigzag pattern (Figures

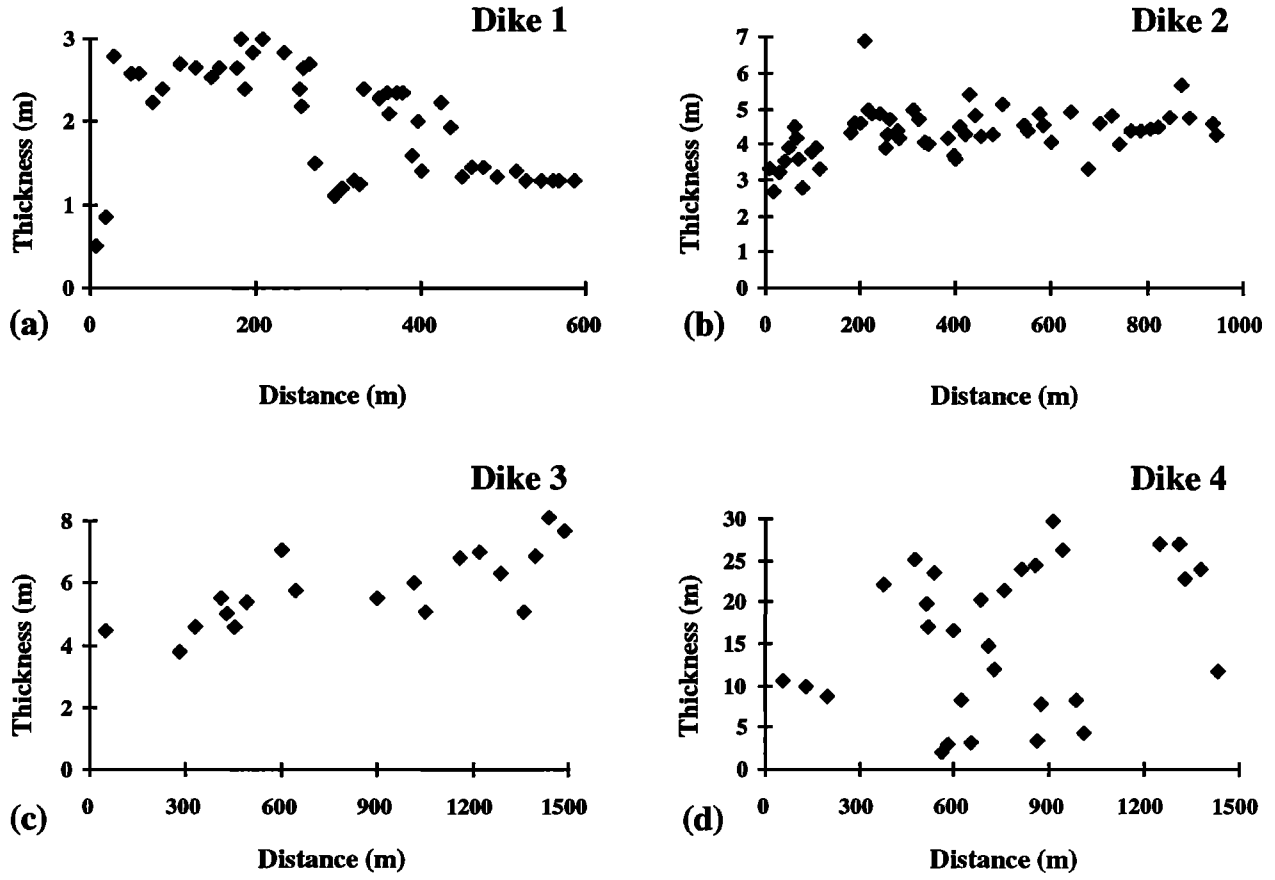

Figure 3. Segment thicknesses along the four Timna dikes.

2c, 2d, 6) associated with preexisting joint systems in the host granite and with the older system of andesitic dikes (Figure 6a). Figure 7 shows the poles to all these segments. A bimodal distribution around two maxima, NNW and NE, corresponds to the attitudes of the major dike sections. Sections 1, 3 and 5 (Figure 5) correspond to the NNW maximum and sections 2, 4, and 6 correspond to the NE maximum.

Reconstruction of the walls of section 4 to their preintrusion position (Figure 6b) by matching the older andesitic dikes on both sides of the doleritic dike enables identification of dilation normal to the NW striking dike walls, and of dextral shear along these walls (Figure 6c). The open gaps in the reconstructed position (Figure 6b) indicate that some wall segments dilated more than others (see later discussion). The reconstruction also indicates that the shear parallel to the walls occurred after the emplacement. The absence of shear structures along other sections of the dike, the occurrence of many other 140^0 striking right-lateral faults in Timna, and their correlation with the Tertiary Dead Sea stress field [*Eyal and Reches*, 1983], suggest that this shear could be due to young faulting unrelated to dike emplacement.

Age Relations of Dikes and Fractures

The attitudes of the segments of the four dikes described above change significantly and abruptly along their strikes (Figures 4, 5). These changes are most likely related to dilation along preexisting fractures of different attitudes. *Delaney et al.* [1986] distinguished between dike-generated joints and preexisting joints by comparing their abundance close to the dike with their regional abundance. Similarly, we determine the age relationships of dikes and fractures in Timna Mountain by examining the relative abundances of fractures and by mapping the crosscutting relations among the dikes and between dikes and fractures.

The oldest sheet structures in Timna Mountain are the N striking rhyolitic dikes and their associated fracture sets. Following in age is the dominant joint set striking generally NE, subparallel to the andesitic dikes. Since the density of this set changes only slightly with the proximity to the andesitic dikes (Figure 6) and since some of the NE striking dikes crosscut these fractures, this set formed either before the NE dikes or semicontemporaneously with them. We therefore envision that the NE striking andesitic dikes encountered a set of joints striking 15^0 to 90^0.

The andesitic dikes were followed by the NW striking doleritic dikes (Figure 6a). At that stage the Timna basement was already disturbed by the joint systems that preceded the NE striking andesitic dikes, as well as by the N striking joints associated with the rhyolitic dikes. The crooked walls of the doleritic dike (dike 4) appear to follow these joints, and in the reconstructed position, many of these joints can be matched on opposite dike walls (Figure 6b). The 130^0-140^0 striking joints, which are subparallel to the major dike sections are considerably less abundant at distances of more than a few meters from the dike. Further, they do not continue into the host granite at the termination zones of the three major NW striking sections (Figure 6). We therefore conclude that the NW striking joints were generated by the doleritic dike, whereas the other joint sets dilated by the doleritic dike existed prior to its emplacement.

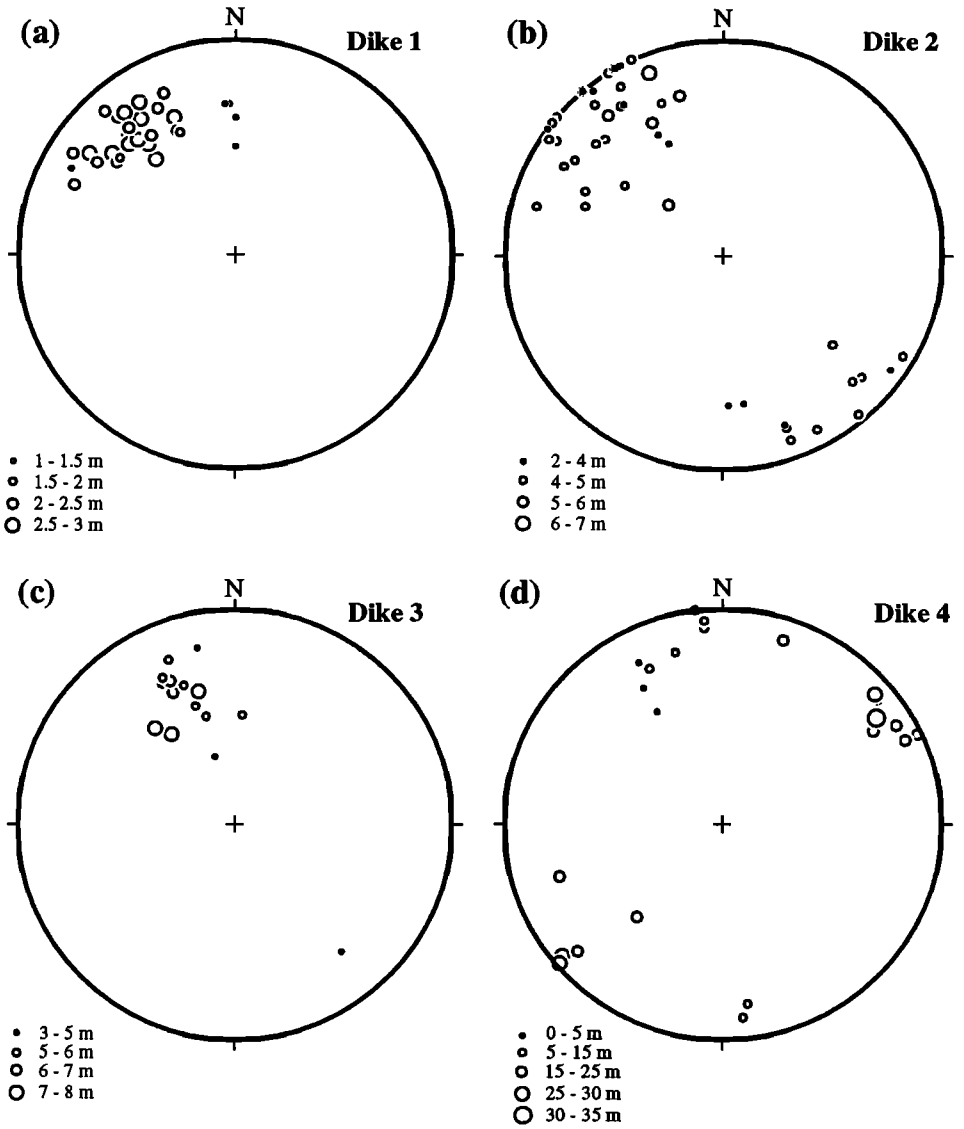

Figure 4. Poles to the measured segments of each of the four dikes, also displaying the thicknesses of these segments. Lower hemisphere, equal-angle stereographic projection.

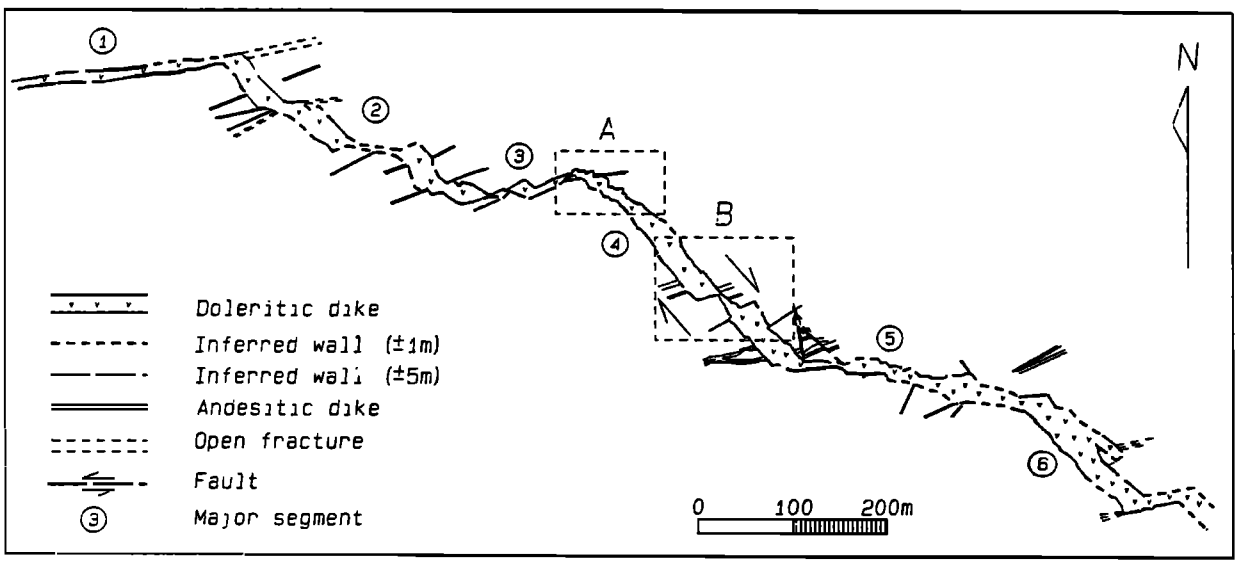

Figure 5. A map of the southeastern part of dike 4, the NW trending doleritic dike. A and B are the sites of Figures 2c, 2d and 6 (reprinted from *Baer and Beyth,* [1990]).

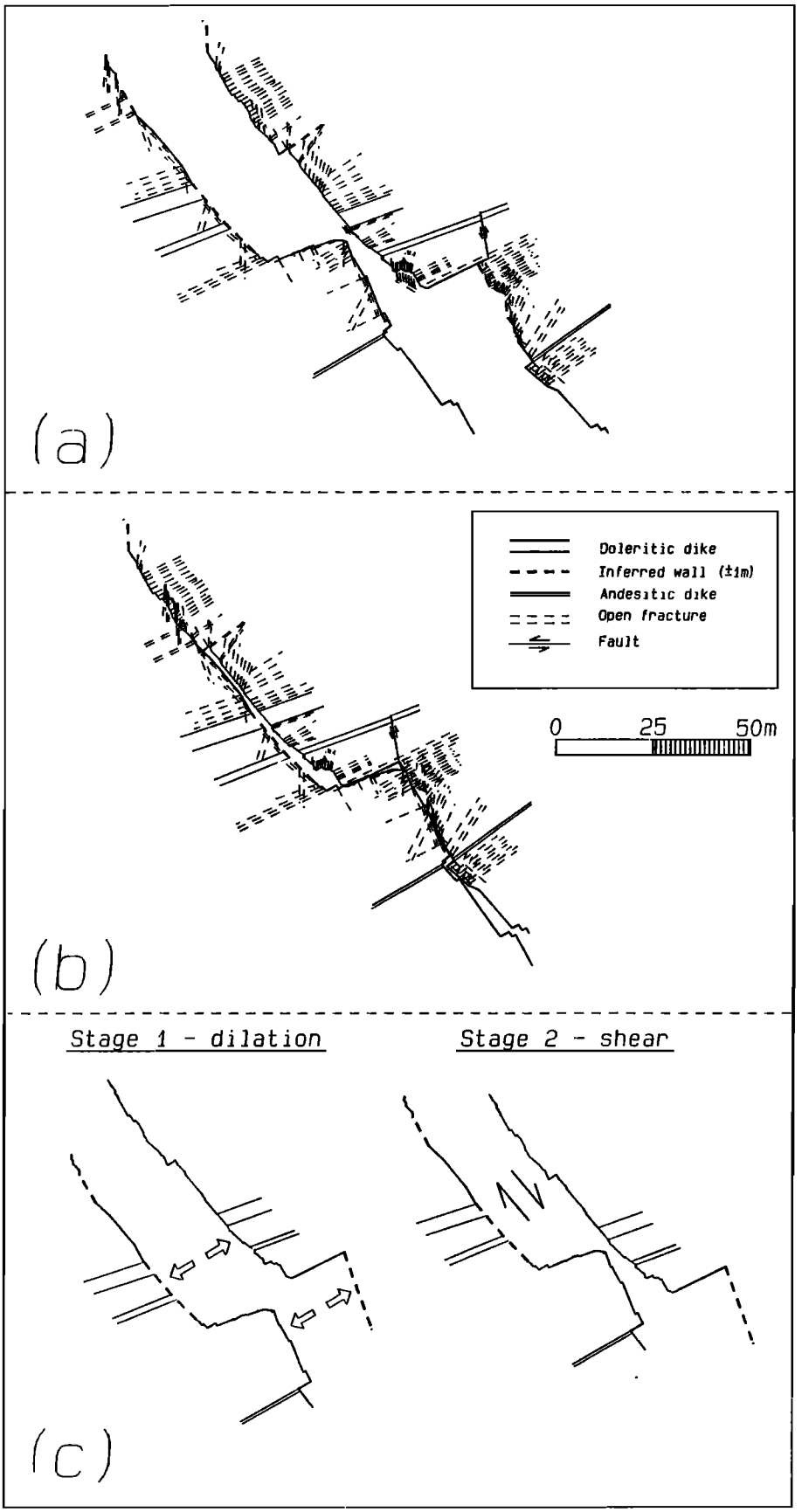

Figure 6. Detailed map of the central part of section 4 of dike 4 (Figure 2d) showing the relations between the dike walls and adjacent structures. (a) Walls at present geometry. (b) Reconstructed to the preintrusion position. (c) Two stages of wall displacement: stage 1, wall-normal dilation; stage 2, wall-parallel shear (reprinted from *Baer and Beyth*, [1990]).

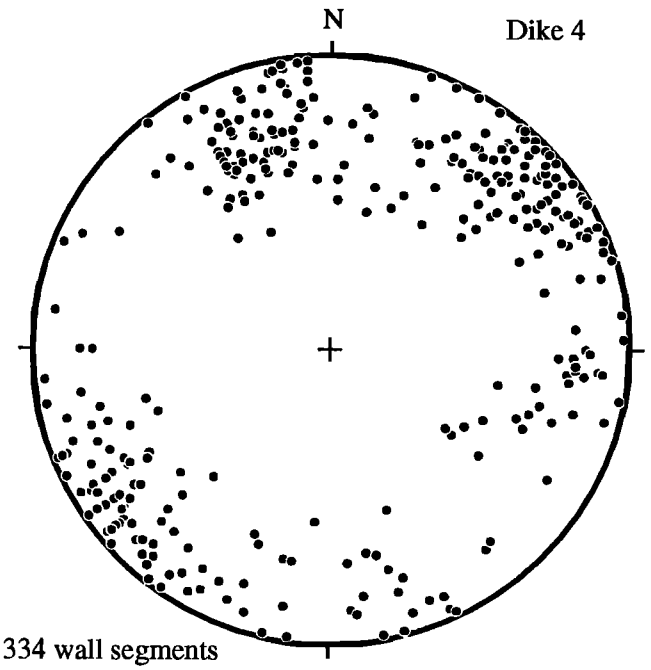

Figure 7. Poles to the contact walls of dike 4. Lower hemisphere stereographic projection.

Dilation of Cracks by Magma

The effect of preexisting fractures on dike geometry is examined here for three styles of initial crack arrays (Figure 8). The first is utilized to infer the stress state and the driving pressure during emplacement. The second and third predict thickness variations along dikes. The three styles are not mutually exclusive, and more than one could describe a given dike. The predictions of the three styles are later compared to the field observations.

Style A: Randomly Oriented Cracks

We first examine a dike emplaced into rock with many preexisting fractures of random orientations. To simplify the solution, we ignore the mechanical interactions of the fractures. Consider a fracture whose normal is inclined to the principal stress axes σ_1, σ_2, σ_3, at angles θ_1, θ_2, and θ_3, respectively . The directional cosines of these angles are $N_1 = \cos\theta_1$, $N_2 = \cos\theta_2$, and $N_3 = \cos\theta_3$. The far-field normal stress σ_n across the fracture is [e.g., *Jaeger and Cook,* 1979, p. 27]

$$\sigma_n = \sigma_1 N_1^2 + \sigma_2 N_2^2 + \sigma_3 N_3^2 . \quad (1)$$

The intruding magma could dilate this fracture if the driving pressure is positive, $P_d = P_m - \sigma_n \geq 0$, where P_m is the magma pressure. By rearranging (1) and by using the relations $N_1^2 + N_2^2 + N_3^2 = 1$, one gets for positive driving pressure

$$\frac{P_m - \sigma_3}{\sigma_1 - \sigma_3} - N_1^2 - \frac{\sigma_2 - \sigma_3}{\sigma_1 - \sigma_3} N_2^2 \geq 0. \quad (2)$$

We define $(P_m - \sigma_3) / (\sigma_1 - \sigma_3)$ as the normalized driving pressure R. This is a convenient ratio to express the relative magnitude of magma pressure with respect to the maximum tectonic shear stress; it is slightly different from the stress ratio R used by *Delaney et al.* [1986] for the two-dimensional analysis of dikes and joints. The stress ratio $\phi = (\sigma_2 - \sigma_3) / (\sigma_1 - \sigma_3)$ indicates the shape of the stress ellipsoid, i.e., the relative magnitude of the intermediate stress σ_2, with respect to the maximum and minimum stresses σ_1 and σ_3 [*Angelier*, 1984; *Reches,* 1987]. Equation (2) can now be written as

$$\frac{1}{R} N_1^2 + \frac{\phi}{R} N_2^2 \geq 1 . \quad (3)$$

Equation (3) is best presented on a stereographic projection with σ_1, σ_2, and σ_3 as its axes (Figure 9). For the bounding case of zero driving pressure and a given pair of R and ϕ ($0 \leq R \leq 1$ and $0 \leq \phi \leq 1$), equation (3) appears as a curve that is symmetric with respect to the principal stress planes (Figure 9). The curve separates between two regions. One includes poles to planes with positive driving pressure, $P_d > 0$ (hatched side of the curves in Figure 9), and the other includes poles to planes with negative driving pressure, $P_d < 0$ (smooth side of the curves in Figure 9). The region with positive driving pressure is centered on σ_3, its half length is θ_L degrees along the σ_3 - σ_2 plane and its half width is θ_W degrees along the σ_3 - σ_1 plane (Figure 9). As an example, for $R = 0.1$ and $\phi = 0.2$ (case b in Figure 9), the half length is $\theta_L = 45^0$ and the half width is $\theta_W = 20^0$. By setting once $N_1 = 0$ and once $N_2 = 0$ in equation (3) (the intersections of the curve with the σ_3-σ_2 and the σ_3-σ_1 planes, respectively), one can show that

$$R = \sin^2 \theta_W \quad (4a)$$

and

$$\phi = \frac{\sin^2 \theta_W}{\sin^2 \theta_L} \quad (4b)$$

The above relations indicate that the projected poles to dilated dike segments should fall in an elongated to equidimensional region on the stereographic projection. A narrow region indicates a low driving pressure ($P_m \sim \sigma_3$) (curve d, Figure 9), whereas a wide region indicates a high driving pressure ($P_m \sim \sigma_1$) (curve e). Similarly, an elongated region indicates a low stress ratio ($\sigma_2 \sim \sigma_3$) (curve a), whereas a circular region indicates a high stress ratio ($\sigma_2 \sim \sigma_1$) (curve c). Further, a pair of θ_W and θ_L corresponds to a unique pair of R and ϕ. These relations are shown in Figure 10b in which the five curves of Figure 9 are marked by open circles.

This analysis provides a simple tool to estimate the state of stress during dike emplacement into a fractured host rock. First, the poles to dilated fractures are plotted on a stereographic projection. Typically, the poles will be restricted to a certain region on the projection (Figures 4, 7). Second, the half width θ_W and half length θ_L of the region are estimated (e.g., $\theta_L = 31^0$, $\theta_W = 16^0$ in Figure 4a). Equations (4) or Figure 10b may be used to determine the stress parameters R and ϕ. Third, the least compressive stress σ_3 should be in the center of the region with poles. The σ_2 axis should be 90^0 from σ_3 in the elongation direction of the region; the σ_1 axis should be 90^0 from the two other stress axes. The orientations of the three principal stress axes are the three eigenvectors associated with the group of projected poles.

Style B: Single crack in a Homogeneous Medium

The second crack configuration is of a single, linear crack in a homogeneous elastic medium (Figure 8). The crack length is $2L$ and it is subjected to a constant internal magma pressure P_m. The elastic medium is subjected to a uniform tectonic stress with a normal stress component σ_n perpendicular to the

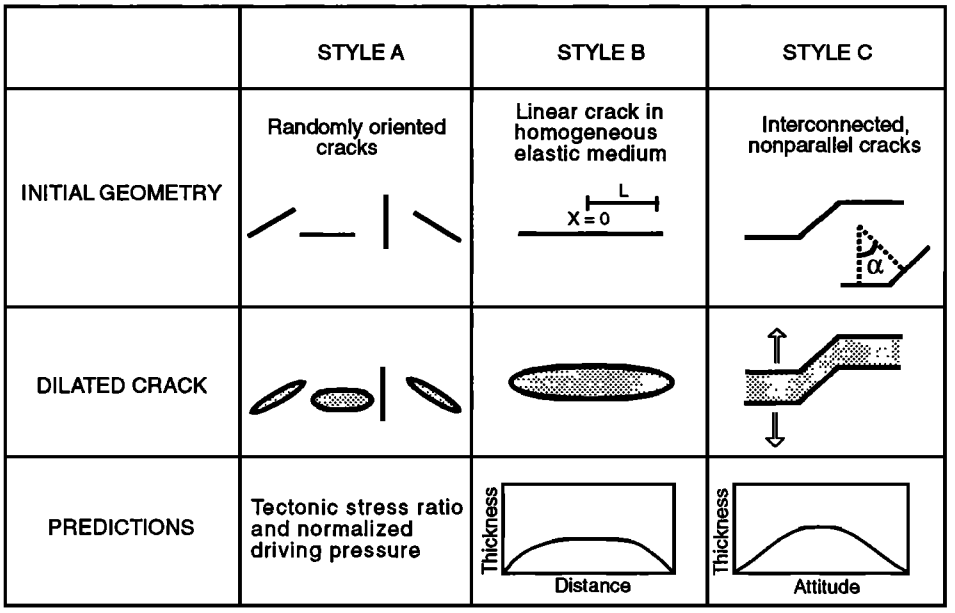

Figure 8. Schematic presentation of three dilation styles of dikes as related to the idealized initial crack geometries. Style A is utilized to infer the stress state and styles B and C predict thickness variations of the dike segments.

dike walls. Under plane-strain conditions the dike dilates to form an elliptical cross section with local thickness $W(x)$,

$$W(x) = 2\,\frac{1-\nu}{\mu}\,(P_m - \sigma_n)\sqrt{L^2 - x^2} \tag{5}$$

where x is the position along the dike, $-L \le x \le L$ (Figure 8), and μ and ν are the shear modulus and Poisson's ratio of the elastic medium [*Pollard et al.*, 1983]. For homogeneous host rock, the maximum thickness of the dike, W_{max}, is at its center (x=0). Substituting W_{max} into (5) yields the thickness relation,

$$\frac{W(x)}{W_{max}} = \sqrt{1 - \frac{x^2}{L^2}}\,. \tag{6}$$

Gradients in the driving pressure along the strike of the dike [*Pollard and Muller,* 1976] and inelastic deformation at the dike tip (process zone) may also affect the thickness profile, leading to deviations from the symmetric ellipse. These effects are neglected from the present analysis to simplify the discussion of our field observations.

Style C: Array of Interconnected Nonparallel Cracks

Consider a dike that dilates a crooked surface composed of an array of interconnected, nonparallel cracks (Figure 8). The blocks on both sides of the dike are regarded as rigid, ignoring their elastic deformation. If this dike dilates in the direction of the least compressive stress, σ_3, a segment that is perpendicular to σ_3 will dilate normal to its walls, whereas the other segments will dilate obliquely [*Baer and Beyth,* 1990]. The thickness $W(\alpha)$ of a given segment that forms an angle α (in three - dimensional space) with the segment of thickness W_{max} that dilates normal to the least compressive stress is

$$W(\alpha) = W_{max} \cos(\alpha). \tag{7}$$

Since the segment thicknesses of each dike are scattered, the values of W_{max} and α are determined in the following way. For each dike, the entire population of segments is scanned in search for a least squares solution of the form

$$LS(D_{max}, S_{max}, W_{max}) = \sum_{i=1}^{N} (W_i^o - W_i^e)^2 \tag{8}$$

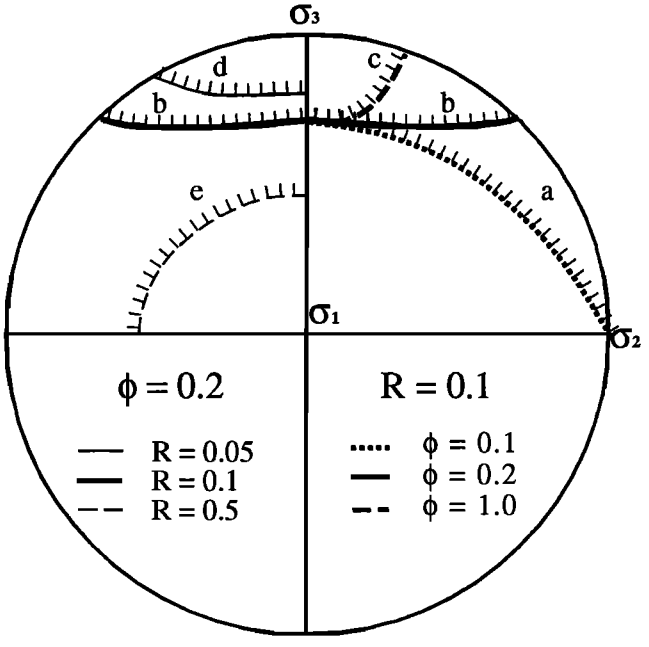

Figure 9. Calculated boundaries of the region of poles to dilated cracks for five different sets of (R,ϕ) (the normalized driving pressure and stress ratio according to equation (4)). The stereographic projection displays only a quarter of each boundary for symmetry considerations. The hatched side of each curve encloses the region of poles to dilated cracks (see text).

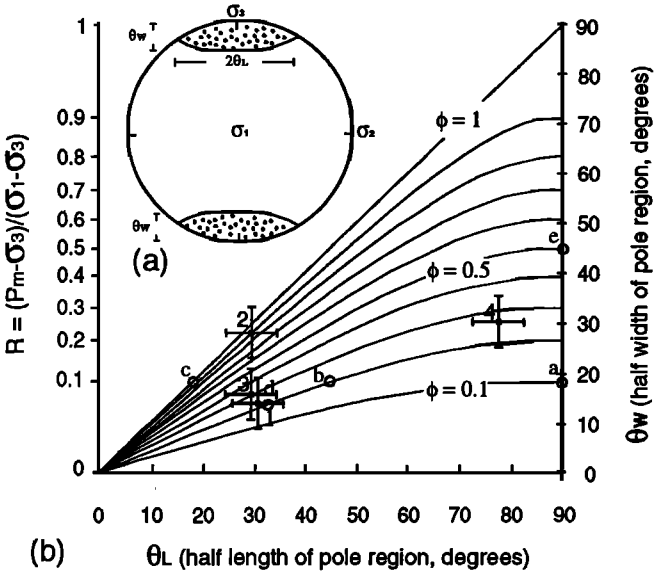

Figure 10. Stress state and driving pressure associated with style A dilation (Figure 8). (a) Stereographic projection and notation for an idealized region of poles to dike segments (see text). (b) The tectonic stress ratio ϕ (fine curves) and the normalized driving pressure R (vertical axis on the left) as determined by the length θ_L and the width θ_W of the region of poles (equation (4)). Squares represent the values inferred for the four Timna dikes; error bars 10^0 by 10^0 in size represent the errors in evaluating θ_L and θ_W. Open circles represent values for five cases used for demonstration (see text and Figure 9).

where D_{max}, S_{max}, and W_{max} are the dip, strike, and thickness of the optimally oriented "thickest" segment, W_i^o is the observed thickness of the i^{th} segment, $W_i^e = W_{max} \cos(\alpha)$, is the expected thickness of this segment, α is the angle between the i^{th} segment and the optimally oriented segment of D_{max} and S_{max}, and N is the number of segments. As the curve $W_{max} \cos(\alpha)$ is calculated by best fit to the entire segment population, the orientation and thickness of the best fit segment could deviate from the orientation and thickness of the actual thickest segment, and its pole could deviate from the center of the pole region.

Interpretation of Field Observations in Timna

Stress State During Dike Emplacement

The variable segment attitudes of the Timna dikes are utilized to determine the orientation of the least compressive stress σ_3 during dike emplacement (Figure 11). We used three methods to determine this orientation that are based on the following assumptions: (1) The thicker segment indicates a higher driving pressure because the thickness of a dike is proportional to its driving pressure (equation (5)). Thus, under constant magma pressure within a dike, the thickest segment formed normal to the least compressive stress. (2) The center of the region of segment poles corresponds to the axis of the least compressive stress as shown above for style A (Figures 9, 10). (3) The least compressive stress is determined by the best fit $W_{max} \cos(\alpha)$ curve of style C (Figure 12). The normal to the attitude of the calculated D_{max} and S_{max} is an estimate of σ_3 orientation. The orientations of the least compressive stress axes for the dikes as determined by the three methods are (Figure 11, Table 1), dike 1, $12^0/316^0 \pm 11.1^0$; dike 2, $10^0/319^0 \pm 6.4^0$; dike 3, $29^0/329^0 \pm 10^0$; and dike 4, $9^0/56^0 \pm 3.3^0$. The mean orientation of σ_3 calculated for the three NE striking dikes is $17^0/321^0 \pm 12.3^0$.

We evaluated the magnitudes of θ_L and θ_W for the four dikes from the stereographic projections of Figure 4 and plotted them on Figure 10b to infer the stress parameters R and ϕ. The values of θ_L and θ_W bear an error of approximately $\pm 5^0$ due to inaccuracy of the measurement in the field and due to plotting extrapolation on the stereonet. The errors of θ_L and θ_W generate corresponding errors in the values of R and ϕ. The values of R, ϕ, and their estimated errors are listed in Table 1. Dikes 1 and 3 were emplaced under a relatively low driving pressure ratio of $R \sim 0.08$; dikes 2 and 4 were emplaced under a higher driving pressure ratio of $R \sim 0.25$. Dikes 1, 3 and 4 were emplaced under a stress ratio of $\phi = 0.2$-0.3; dike 2 was emplaced under a considerably higher stress ratio of $\phi \sim 0.9$. Dikes 1 and 3 of the NE striking system were emplaced under similar stress states (as reflected in their similar R and ϕ), and both propagated subhorizontally. Dike 2, of the same system, and dike 4, of the NW striking system, propagated vertically, and were emplaced under higher R.

Several previous works evaluated the factors which control the propagation direction of dikes [e.g., *Rubin and Pollard*, 1987; *Baer and Reches*, 1991]. The considered factors are the geometry of the dike, including size, shape, and depth beneath the Earth's surface, and the driving pressure distribution, including the distribution of magma pressure within the dike and of the remote stress acting perpendicular to the dike plane. The Timna dikes appear to suggest an additional factor. On one hand, we found no evidence for major differences in size, shape

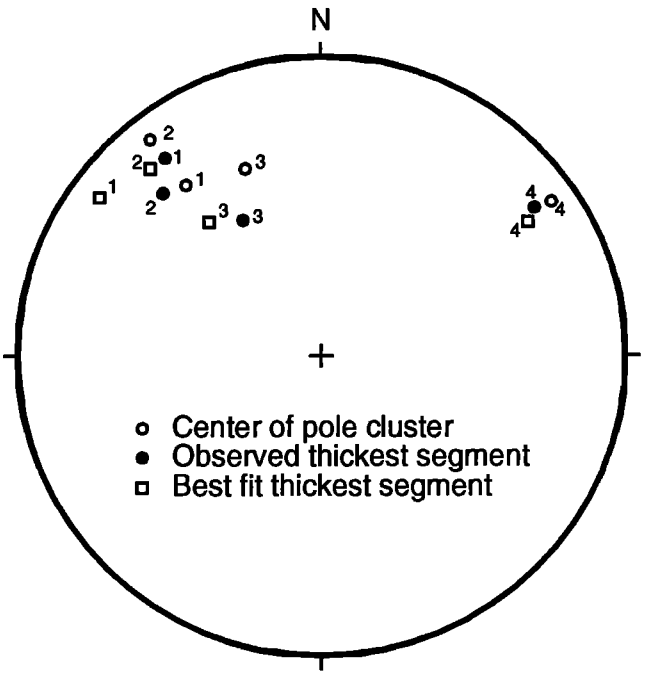

Figure 11. The orientations of the least compressive stress inferred for the four Timna dikes by the center of the region of poles (open circles), by the normal to the thickest segments (solid circles), and by the normal to the best fit thickest segment (open squares).

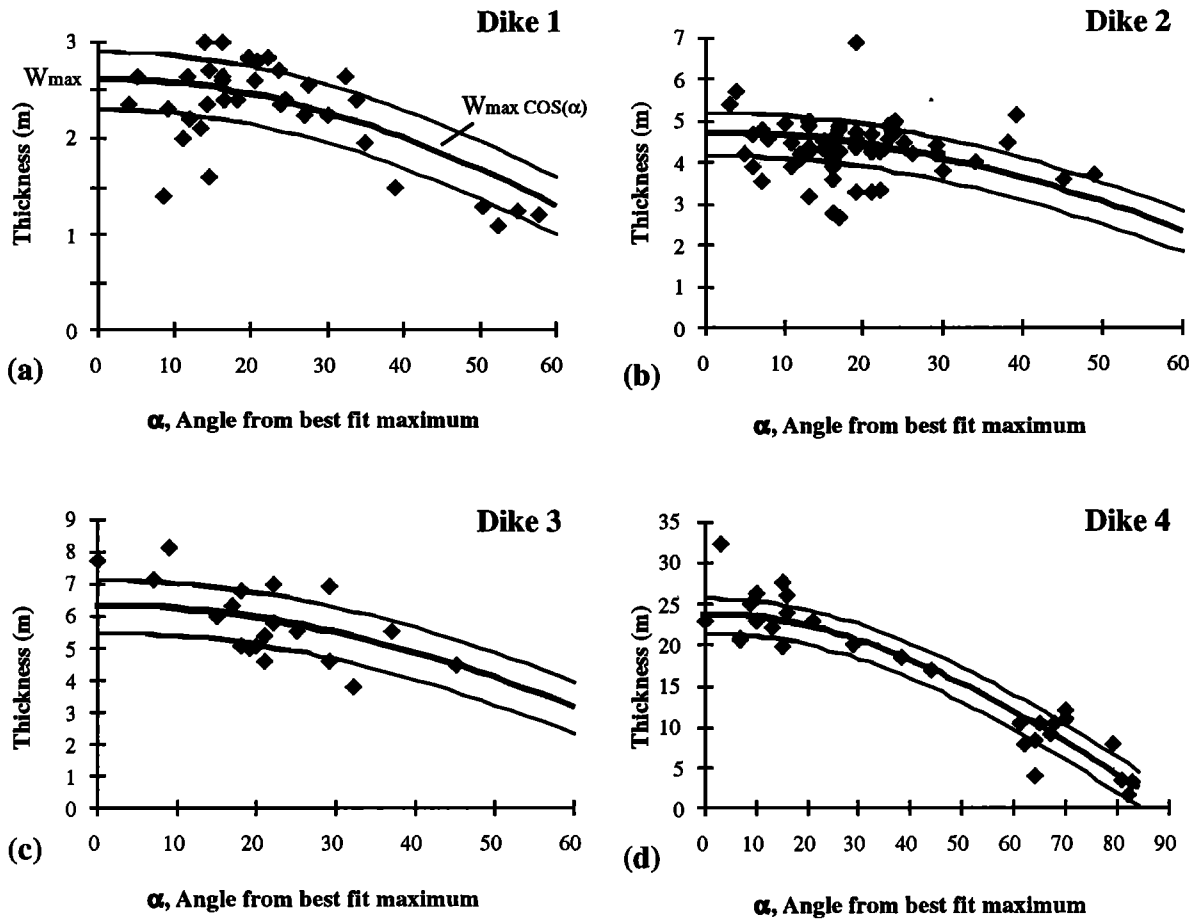

Figure 12. The measured thicknesses of the Timna dikes (solid diamonds) and the predicted thickness according to style C (thick curve) plotted versus the angle between the best fit thickest segment and each of the measured segments (equation (8)). The two thin curves represent ±1 mean deviation for the predicted thickness.

and emplacement depth among the three NE striking Timna dikes (the NW striking dike is considerably thicker than the others). On the other hand, the propagation directions of the NE striking dikes are dissimilar. The apparent correlation that we found between R and the propagation directions suggest that the propagation of these dikes was controlled by the overpressure in their feeding magma chambers, and not by their geometry. A higher driving pressure could indicate a greater magma overpressure in the source region, which is consistent with vertical magma propagation, whereas a low magma overpressure is in accordance with the subhorizontal propagation.

The NE striking Timna dikes are part of a large province of dikes of similar attitudes and compositions that extends from the Eastern Desert in Egypt to northern Saudi Arabia [e.g., *Vail*, 1970]. The regional dike swarms, as well as independent tectonic and stratigraphic evidence, indicate that the crust in this area was actively extending at the Late Precambrian time in a NW-SE direction [*Stern et al.*, 1984]. The present analysis of the emplacement of the Timna dikes provides the first detailed estimate of the tectonic stress state for the northeastern part of the Pan-African basement during the Late Precambrian. If our structural analysis of the Timna dikes is regionally applicable, it suggests that the NE striking dike

Table 1. The Orientations of the Least Compressive Stress Axes Determined by Three Different Methods, and the Tectonic Stress Ratio, and Normalized Driving Pressure for the Four Timna Dikes

	Orientation of the Least Compressive Stress Axis, deg			ϕ	R
Dike	Thickest Segment	Pole Region	Best Fit Curve	Stress Ratio[a]	Driving Pressure[b]
1	10/322	18/322	6/306	0.23±0.17	0.075±0.03
2	16/316	5/322	10/318	0.9±0.25	0.23±0.07
3	35/330	22/338	30/320	0.31±0.21	0.085±0.04
4	9/55	5/56	12/57	0.27±0.09	0.25±0.08

[a] $\phi = (\sigma_2 - \sigma_3)/(\sigma_1 - \sigma_3)$.

[b] $R = (P_m - \sigma_3)/(\sigma_1 - \sigma_3)$.

swarms were emplaced in fractured basement rocks with considerable strike variations of these fractures. The prevailing direction of the least compressive stress σ_3 is subhorizontal, trending NW-SE (Figure 11). The orientations of the other principal stresses σ_1 and σ_2 interchange within a vertical plane normal to σ_3. The accurate stress directions associated with a given dike cannot be simply inferred from the general trend of the dike; they should be determined in one of the methods proposed here.

Thickness Variations

The dilation styles B and C are now applied to the Timna dikes. The single crack dilation style (B) predicts that the thickness is determined by the position along the dike (equations (5) and (6)). The only dike examined that is in partial agreement with such geometry is dike 3 (Figure 3c), which shows a gradual thickening along its strike, from its southwestern end to its northeastern end. The other three dikes do not show any correlation with the predicted thickness of style B. The thicknesses of dikes 1 and 4 vary inconsistently along their strike (Figures 3a, 3d); dike 2 was truncated by faulting, the positions of its tips are unknown, and thus it is not justified to compare its thickness variations with the ellipse of style B.

Figure 12 displays the observed and the predicted thicknesses according to the dilation style C. The figure shows the thickness of the dike segments versus the angle α, and the best fit solutions $W_{max} \cos(\alpha)$ that were calculated as described above (equation (8)). It also shows two curves of the mean deviations from the best fit solution, $\Sigma |W_i^o - W_i^e| / N$. The best correlation between dike thickness and attitudes is displayed by dike 4 (Figure 12d). One may note several segments that are anomalously thicker by 3-10 m than the calculated W_{max} of dike 4 (Figure 12d). We envision that this group, that strikes 130°-140°, dilated and propagated in early stages of dike emplacement until they were arrested by preexisting 60°-90° striking fractures. After their arrest, the differently striking segments of the dike were interconnected and dilated as one dike according to style C. The anomalously thick segments can also be identified in the reconstructed position of Figure 6b as unjuxtaposed walls that require excess movement to totally close the dike.

The emplacement of dike 4 may thus be separated into two stages: (1) formation and dilation of individual, nonconnected NW striking crack segments until they were arrested by the preexisting fractures or dikes, (2) dilation of the interconnected dike segments in a direction perpendicular to the 140° striking segments (and oblique to the 60°-90° striking segments).

The other three dikes display more complicated patterns. Dikes 1 and 3 show a fair correlation between the attitudes of their segments and their thickness (Figures 12a, 12c). Dike 2 shows poor systematic thickness variations with its segments' attitudes (Figure 12b).

In summary, thickness variations in dikes 1, 3, and 4 are fairly well correlated with the attitudes of the dikes' segments (style C dilation), whereas the thickness variations of dike 2 are less defined. Only dike 3 displays correlation between thickness and position along the dike (style B dilation).

Summary and Conclusions

We described here one doleritic dike and three andesitic dikes that intruded the fractured basement of Timna Mountain, Israel. The study demonstrates that dike shapes can be significantly more irregular than commonly envisioned. They may invade a wide range of fracture systems and form segments with large and abrupt thickness variations. This irregular geometry has been utilized to determine several components of the paleostress state and to distinguish between alternative dilation styles. The direction of the least compressive stress during the emplacement of each of the Timna dikes was inferred by three methods: the normal to its thickest segment, the normal to the mean orientation of the dike segments, and the best fit solution of the expected segment thicknesses (according to an interconnected crack dilation style). The results of the three methods agree well with each other (Table 1). The tectonic stress ratio $\phi = (\sigma_2 - \sigma_3)/(\sigma_1 - \sigma_3)$ and the normalized driving pressure $R = (P_m - \sigma_3) / (\sigma_1 - \sigma_3)$ were calculated by analysis of the group of fractures that were dilated by magma to form the dike. The projection of the poles to these fractures is restricted to a certain region on a stereographic projection. The length and width (in degrees) of this region determine the stress ratio and the normalized driving pressure (Figure 10).

The thickness variations along the dikes were compared to the predictions of two styles of initial crack geometry. The first is a single linear crack in a homogeneous elastic medium that grows into an elliptical dike (equation (6) of style B), and the second is an interconnected array of nonparallel cracks that grow into a dike in which the thickness of each segment is related to its attitude by cosine relations (equation (7) of style C). The predictions of the first are met only in one dike, in part because the locations of the dike terminations are unknown. The predictions of the second are in good agreement with the observations of the doleritic dike; several anomalously thick segments of the dike suggest that these segments dilated separately before the dilation of the entire dike. Two of the andesitic dikes show fairly good correlation between attitude and their thickness, while the third dike shows poor thickness-attitude correlation.

The analysis presented in this study could be applied to detect temporal and geographic changes of the stress state in large dike provinces, such as the dike swarms of the Late Precambrian East African-Arabian basement. The present method can also be used to determine the stress state associated with other tensional features such as veins and joints.

Acknowledgments. Many thanks to Alan Rubin and Paul Delaney for their careful reviews and helpful comments on earlier versions of this paper, and to Shlomo Ashkenazi for his assistance in the field. The stereographic projections were made with the "Stereonet" program, written by R.W. Allmendinger.

References

Anderson, E.M., *The Dynamics of Faulting and Dyke Formation With Application to Britain*, 206 pp., Oliver and Boyd, Edinburgh, 1951.

Angelier, J., Tectonic analysis of fault slip data sets, *J. Geophys. Res.*, *89*, 5835-5848, 1984.

Baer, G., Mechanisms of dike propagation in layered rocks and in massive, porous sedimentary rocks, *J. Geophys. Res.*, *96*, 11,911-11,929, 1991.

Baer, G., and M. Beyth, A mechanism of dyke segmentation in fractured host rock, in *Mafic Dykes and Emplacement Mechanisms, Proceedings of the Second International Conference, Adelaide, South Australia, 12-15 September 1990*, edited by A. J. Parker, P. C. Rickwood, and D. H. Tucker, pp. 3-11, Hfl. 170/US$95.00, A.A. Balkema, P.O. Box 1675, Rotterdam, Netherlands, 1990.

Baer, G., and Z. Reches, Mechanics of emplacement and tectonic implications of the Ramon dike systems, Israel, *J. Geophys. Res., 96*, 11,895-11,910, 1991.

Bentor, Y.K., Petrographical outline of the Precambrian in Israel, *Bull. Res. Counc. Isr., Sect. G, 10*, 19-63, 1961.

Beyth, M., and S. Peltz, Petrology and major-element geochemistry of dikes at Har Timna, southern Israel, *Rep. GSI/13/92*, Geol. Surv. of Isr., Jerusalem, 1992.

Delaney, P.T., D.D. Pollard, J.I. Ziony, and E.H. McKee, Field relations between dikes and joints: Emplacement processes and paleostress analysis, *J. Geophys. Res., 91*, 4920-4938, 1986.

Eyal, Y., and Z. Reches, Tectonic analysis of the Dead Sea Rift region since the Late Cretaceous based on mesostructures, *Tectonics, 2*, 167-185, 1983.

Jaeger J.C., and N.G.W. Cook, *Fundamentals of Rock Mechanics*, 593 pp., Chapman and Hall, London, 1979.

Kroner, A., and M. Beyth, Single Zircon ages for Late Precambrian magmatic rocks of Har Timna, *Isr. Geol. Soc. Ann. Mtg., Elat*, 51, 1990.

Pollard, D.D., Derivation and evaluation of a mechanical model for sheet intrusions, *Tectonophysics, 19*, 233-269, 1973.

Pollard, D.D., and O.H. Muller, The effect of gradients in regional stress and magma pressure on the form of sheet intrusions in cross section, *J. Geophys. Res., 81*, 975-984, 1976.

Pollard, D.D., O.H. Muller, and D.R. Dockstader, The form and growth of fingered sheet intrusions, *Geol. Soc. Am. Bull., 86*, 351-363, 1975.

Pollard, D.D., P.T. Delaney, W.A. Duffield, E.T. Endo, and A.T. Okamura, Surface deformation in volcanic rift zones, *Tectonophysics, 94*, 541-584, 1983.

Reches, Z., Determination of the tectonic stress tensor from slip along faults that obey the Coulomb yield condition, *Tectonics, 6*, 849-861, 1987.

Rubin, A.M., and D.D. Pollard, Origins of blade-like dikes in volcanic rift zones, *U.S. Geol. Surv. Prof. Pap., 1350*, 1449-1470, 1987.

Schurmann, H.M.E., *The Precambrian Along the Gulf of Suez and the Northern Part of the Red Sea*, 404 pp., E. J. Brill, Leiden, Netherlands, 1966.

Shafranek, D., Dykes in the south eastern part of the Precambrian massif of Sinai, The Hebrew Univ. of Jerusalem, (in Hebrew, with English summary), M.Sc. thesis, 99 pp., 1978.

Stern, R.J., D. Gottfried, and C.E. Hedge, Late Precambrian rifting and crustal evolution in the northeastern Desert of Egypt, *Geology, 12*, 168-172, 1984.

Vail, J.R., Tectonic control of dykes and related irruptive rocks in eastern Africa, in *African Magmatism and Tectonics*, edited by T.N. Clifford and I.G. Gass, pp. 337-354, Oliver and Boyd, Edinburgh, 1970.

Zlatkine, A., and U. Wurzburger, Eruptive rocks of Timna (Negev), *Bull. Geol. Surv. Isr., 14*, 41 pp., 1957.

G. Baer and M. Beyth, Geological Survey of Israel, 30 Malkhe Yisrael St., Jerusalem 95501, Israel. (e-mail: baer@vms.gsi.gov.il)

Z. Reches, Department of Geology, Hebrew University, Jerusalem 91904, Israel. (e-mail: reches@vms.huji.ac.il)

(Received March 10, 1993; revised August 9, 1994;
accepted August 15, 1994.)